Materials Science and Engineering A 554 (2012) 67–71

Contents lists available at SciVerse ScienceDirect

Materials Science and Engineering A

journal homepage: www.elsevier.com/locate/msea

Effective elastic properties of polycrystals based on phase-field description

G. Sheng[a,*], S. Bhattacharyya[a], H. Zhang[a], K. Chang[a], S.L. Shang[a], S.N. Mathaudhu[b], Z.K. Liu[a], L.Q. Chen[a]

[a] Department of Materials Science and Engineering, The Pennsylvania State University, University Park, PA 16802, USA
[b] Materials and Manufacturing Sciences Division, U.S. Army Research Laboratory, Aberdeen Proving Ground, MD 21005, USA

ARTICLE INFO

Article history:
Received 18 April 2012
Received in revised form 4 June 2012
Accepted 6 June 2012
Available online 15 June 2012

Keywords:
Phase-field models
Magnesium
Simulation
Elastic behavior
Polycrystal

ABSTRACT

A combination of microelasticity, phase-field description of grain structures, and first-principles calculations is proposed to predict the effective elastic properties of polycrystals. As an example, using the single crystal elastic constants from first-principles calculations and a polycrystalline microstructure from a phase-field simulation as inputs, the effective elastic moduli of polycrystalline magnesium are obtained as a function of temperature and compared with available experimental measurements. The texture effect on the effective elastic moduli is also examined. The proposed integrated model will make it possible to model not only the temporal evolution of microstructures but also the temporal evolution of properties using the phase-field method.

1. Introduction

As lightweight structural materials with a good combination of castability and mechanical properties, magnesium alloys receive substantial interest for potential transportation applications such as the automobile body materials for weight reduction and higher fuel efficiency [1,2]. Elastic properties of magnesium and its alloys have been extensively studied in the last several decades. For example, the elastic stiffness tensor of single crystal Mg was determined through both experimental measurements [3–6] as well as theoretical predictions [7,8]. However, most practical magnesium alloys are polycrystalline materials, and the overall elastic stiffness tensor depends on the orientation of each grain constituting the polycrystal. The distribution of crystallographic orientations, or texture, will significantly affect the effective elastic properties of a polycrystalline. For magnesium alloys, typical textures include the recrystallization texture which forms during the solidification process and the deformation texture which forms during the rolling of magnesium sheets [9].

Modeling the effective elastic modulus was pioneered by Voigt [10], Reuss [11] and Hill [12], who proposed a useful scheme by which one calculates isotropic polycrystalline elastic moduli in terms of the anisotropic single crystal elastic constants. Dutta et al. [13] reported the effective elastic properties of polycrystalline Cu, Ni, Al and Ag, using an extended Green function approach. This approach was also applied to determine the effective elastic properties of spinel, rutile, Al, AgCl and ZnO [14]. The method reported by Kiewel et al. [15,16] solved the elastic displacement equation in a cluster of 100–1000 grains subjected to a homogeneous deformation. Satisfactory agreements are achieved between their calculations and experimental values in a wide range of cubic, tetragonal and hexagonal materials. In composite materials like multilayer ceramic capacitor (MLCC), finite element method is also employed to calculate the effective modulus [17].

During the last two decades, the phase-field method [18] has emerged as a powerful tool to model complicated microstructure evolution across many fields. Recently there have been efforts to predict the effective properties of multiphase materials by combining phase-field representation of microstructures and homogenization approach. Ni and Chiang [19] adapted the phase-field microelasticity method into the homogenization process to estimate the effective elastic constants of 3D heterogeneous (multiphase) materials with both intermingled and dispersed phases. Laschet and Apel [20] developed a similar multi-scale approach based on the asymptotic homogenization method of periodic material structures to calculate the effective cubic Young's and shear moduli and Poisson coefficients in a ferrite/austenite dual-phase steel with different ferrite volume fractions.

Recently, Bhattacharyya et al. [21,22] developed an effective phase-field approach based on the iterative-perturbation method [23] to compute the residual stress distributions in polycrystalline materials with arbitrary inhomogeneous distributions of elastic moduli. Using this method, the effective elastic properties of the polycrystalline material can be efficiently computed from its

* Corresponding author at: Scientific Forming Technologies Corporation, Columbus, OH 43235, USA. Fax: +1 614 451 8325.
E-mail address: shengguang1982@gmail.com (G. Sheng).

0921-5093/$ – see front matter © 2012 Elsevier B.V. All rights reserved.
http://dx.doi.org/10.1016/j.msea.2012.06.012

response to an applied strain or stress. In this paper, we will employ this approach to compute the effective elastic constants of polycrystalline magnesium, using single crystal elastic constants and a 3D polycrystalline microstructure from phase-field simulation as inputs. The derived effective elastic moduli from the calculated elastic constants will be compared with available experimental measurements. We will also investigate the effective elastic properties as a function of texture, by specifying the orientations of certain amount of grains from 0% (fully random distribution) to 100% (fully textured). Typical fiber and basal textures in hexagonal materials, especially in polycrystalline magnesium will be selected as examples.

2. Model

In the phase-field model of grain growth [24–27], a polycrystalline microstructure is described using a set of Q continuous, non-conserved order parameter fields $\eta_i(\mathbf{r}, t)$ $(i = 1 \cdots Q)$. The order parameter fields represent grains of a given crystallographic orientation. A monitor function $\phi(\mathbf{r}, t) = \sum_i \eta_i^2(\mathbf{r}, t)$ is used to distinguish between the grain interior and the grain boundaries [24,25]. Since the grains are rotated with respect to a fixed coordinate system, the elastic stiffness tensor for each grain is obtained by transforming the tensor with respect to the fixed coordinate system. Let C_{ijkl} represents the stiffness tensor for a single grain in a fixed reference frame. Then, the position-dependent elastic stiffness tensor $C_{ijkl}(\mathbf{r})$ for the entire polycrystal in terms of the order parameter fields is given by

$$C_{ijkl}(\mathbf{r}) = \sum_g \eta_g^2(\mathbf{r}) a_{ip}^g a_{jq}^g a_{kr}^g a_{ls}^g C_{pqrs}, \tag{1}$$

where C_{pqrs} is the stiffness tensor of the fixed reference frame, a_{ij}^g is the transformation matrix representing the rotation of the coordinate system defined on a given grain g with respect to the fixed reference frame and is expressed in terms of the Euler angles θ, ψ, and ζ as follows:

$$a_{ij}^g = \begin{pmatrix} \cos\theta\cos\zeta - \sin\theta\sin\zeta\cos\psi & \sin\theta\cos\zeta + \cos\theta\sin\zeta\cos\psi & \sin\zeta\sin\psi \\ -\cos\theta\sin\zeta - \sin\theta\cos\zeta\cos\psi & -\sin\theta\sin\zeta + \cos\theta\cos\zeta\cos\psi & \cos\zeta\sin\psi \\ \sin\theta\sin\psi & -\cos\theta\sin\psi & \cos\psi \end{pmatrix}, \tag{2}$$

where $0 \le \theta \le 2\pi$, $0 \le \psi \le \pi$, $0 \le \zeta \le 2\pi$.

The elastic stiffness tensor $C_{ijkl}(\mathbf{r})$ varying in space can be considered as made up a homogeneous part C_{ijkl}^0 and an inhomogeneous perturbation $C'_{ijkl}(\mathbf{r})$

$$C_{ijkl}(\mathbf{r}) = C_{ijkl}^0 + C'_{ijkl}(\mathbf{r}). \tag{3}$$

Thus $C_{ijkl}(\mathbf{r})$ can also be rewritten as

$$C_{ijkl}(\mathbf{r}) = C_{ijkl}^0 + \left(\sum_g \eta_g^2(\mathbf{r}) a_{ip}^g a_{jq}^g a_{kr}^g a_{ls}^g C_{pqrs} - C_{ijkl}^0 \right). \tag{4}$$

Let $\epsilon_{ij}(\mathbf{r})$ denotes the total strain measured with respect to a reference undeformed lattice. Then, assuming linear elasticity, the local stress $\sigma_{ij}(\mathbf{r})$ is given by

$$\sigma_{ij}(\mathbf{r}) = (C_{ijkl}^0 + C'_{ijkl}(\mathbf{r}))(\epsilon_{kl}(\mathbf{r}) - \epsilon_{kl}^0(\mathbf{r})), \tag{5}$$

where $\epsilon_{ij}^0(\mathbf{r})$ is the position-dependent eigenstrain given by $\epsilon_{ij}^0(\mathbf{r}) = \sum_g \eta_g^2(\mathbf{r}) a_{ip}^g a_{jq}^g \epsilon_{pq}^{0,g}$, where $\epsilon_{pq}^{0,g}$ is the eigenstrain associated with grain 'g'.

To obtain the local elastic field, we solve the mechanical equilibrium equation

$$\frac{\partial \sigma_{ij}}{\partial r_j} = 0, \quad \text{i.e. } \nabla_j C_{ijkl}(\mathbf{r})(\epsilon_{kl}(\mathbf{r}) - \epsilon_{kl}^0(\mathbf{r})) = 0. \tag{6}$$

The total strain $\epsilon_{ij}(\mathbf{r})$ can be expressed as a sum of homogeneous and heterogeneous strains:

$$\epsilon_{ij}(\mathbf{r}) = \bar{\epsilon}_{ij} + \delta\epsilon_{ij}(\mathbf{r}), \tag{7}$$

where the homogeneous strain $\bar{\epsilon}_{ij}$ is defined so that

$$\int \delta\epsilon_{ij}(\mathbf{r}) d^3 r = 0. \tag{8}$$

The heterogeneous strain field $\delta\epsilon_{ij}(\mathbf{r})$ is defined as

$$\delta\epsilon_{ij}(\mathbf{r}) = \frac{1}{2}\left(\frac{\partial u_i(\mathbf{r})}{\partial r_j} + \frac{\partial u_j(\mathbf{r})}{\partial r_i} \right), \tag{9}$$

where $u_i(\mathbf{r})$ denotes the ith component of displacement field.

Substituting Eqs. (7) and (9) into Eq. (6), we obtain

$$\nabla_j C_{ijkl}(\mathbf{r}) \left[\bar{\epsilon}_{kl} + \frac{1}{2}\left(\frac{\partial u_k(\mathbf{r})}{\partial r_l} + \frac{\partial u_l(\mathbf{r})}{\partial r_k} \right) - \epsilon_{kl}^0(\mathbf{r}) \right] = 0. \tag{10}$$

Substituting Eq. (4) into Eq. (10) and simplifying, we obtain

$$C_{ijkl}^0 \frac{\partial^2 u_k(\mathbf{r})}{\partial r_j \partial r_l} = \nabla_j \left\{ \left(\sum_g \eta_g^2(\mathbf{r}) a_{ip}^g a_{jq}^g a_{kr}^g a_{ls}^g C_{pqrs} \right) (\epsilon_{kl}^0(\mathbf{r}) - \bar{\epsilon}_{kl}) \right\} - \frac{\partial}{\partial r_j} \left[\left(\sum_g \eta_g^2(\mathbf{r}) a_{ip}^g a_{jq}^g a_{kr}^g a_{ls}^g C_{pqrs} - C_{ijkl}^0 \right) \frac{\partial u_k(\mathbf{r})}{\partial r_l} \right]. \tag{11}$$

For a given homogeneous strain and an eigenstrain distribution, Eq. (11) can be solved by the efficient iterative perturbation scheme [21,22] to obtain the local stress distribution $\sigma_{ij}(\mathbf{r})$. The average stress in the polycrystalline material σ_{ij}^{av} is then calculated as

$$\sigma_{ij}^{av} = \frac{1}{V}\int_V \sigma_{ij}(\mathbf{r}) \mathrm{dV}. \tag{12}$$

When the system is subjected to a constant strain field, the homogeneous strain $\bar{\epsilon}_{ij}$ is equal to the applied strain. The effective elastic stiffness tensor C_{ij}^{eff} (in Voigt notation) can be obtained by the following equation

$$\sigma_i^{av} = C_{ij}^{eff} \bar{\epsilon}_j. \tag{13}$$

After C_{ij}^{eff} is obtained, the bulk modulus (B), shear modulus (G) and Young's modulus (E) can be calculated by $B = (\bar{C}_{11} + 2\bar{C}_{12})/3$, $G = (\bar{C}_{11} - \bar{C}_{12} + 3\bar{C}_{44})/5$ and $E = (9BG)/(G + 3B)$, where $\bar{C}_{11} = (C_{11} + C_{22} + C_{33})/3$, $\bar{C}_{12} = (C_{12} + C_{13} + C_{23})/3$, and $\bar{C}_{44} = (C_{44} + C_{55} + C_{66})/3$.

In all the following calculations, the effective elastic moduli are calculated using two different treatments of the grain boundaries: sharp interface and diffuse interface. The sharp interface model assumes the elastic modulus changing sharply across the grain boundaries, and the excess volume associated with the grain

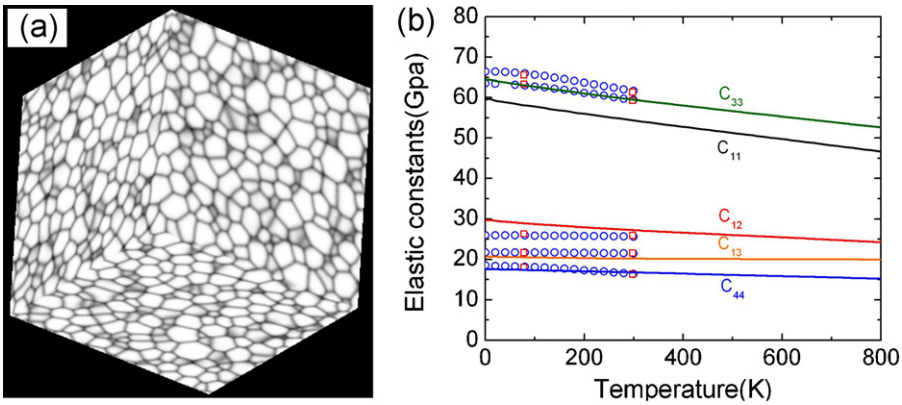

Fig. 1. (a) A 3D polycrystalline microstructure generated from phase-field simulations. (b) Temperature dependent elastic constants of Mg from first-principle calculations [29]. (○) [4] and (□) [5] represent the experimental elastic constants of single crystal Mg.

boundaries is neglected. Therefore, there is neither volume difference nor modulus difference between the grain boundaries and the interior. The sharp interface model is valid when the volume fraction of the grain boundaries in the polycrystalline is small and the average grain size is large (of the order of microns). On the other hand, when the volume fraction of the grain boundaries is high, i.e. average grain size of the order of nanometers, the effect of the grain boundaries on the effective modulus should be taken into account. In this case we employ the diffuse interface model by assuming the elastic moduli vary smoothly across a grain boundary. Furthermore, the grain boundaries are assumed to be elastically softer regions than the grain interior. In our model this assumption is guaranteed by the monitor function $\phi(\mathbf{r}, t) = \sum_i \eta_i^2(\mathbf{r}, t)$ which has the value 1.0 within grains and significantly smaller values (0.5–0.8) at grain boundaries, which makes much smaller elastic moduli at grain boundaries. In the diffuse interface model the volume difference between the grain boundaries and grain interior is also neglected due to the lack of experimental data.

3. Results and discussion

Fig. 1 shows the inputs for the calculation of effective elastic constants of polycrystalline Mg. Fig. 1(a) is a 3D polycrystalline microstructure generated from phase-field grain growth simulation. The simulation uses a $160 \times 160 \times 160$ system size with 10,000 order parameters [26,27]. The order parameter evolution during grain growth was computed through the active parameter tracking (APT) algorithm [27,28] by only picking up the non-zero order parameters. Single crystal Mg elastic constants could be either from first-principles calculations or experimental values if available. In Fig. 1(b) we plot the elastic constants from first-principles calculations as a function of temperature [29] (shown as lines), which has a fairly good agreement with the experimental data between 0 and 300 K [4,5] (shown as points). Using the first-principle data as input, we are able to calculate the effective elastic properties in a wide temperature range from 0 to 800 K.

Table 1
Calculated effective elastic constants of polycrystalline Mg compared with literature data [30].

	C_{11}	C_{12}	C_{13}	C_{33}	C_{44}
This work	58.51	24.27	23.60	60.40	16.81
Ref. [30]	58.58	24.22	24.35	59.58	17.27

Following the method described above, we calculate the effective elastic constants of polycrystalline Mg with fully random grain orientations and compare them with a previous calculation performed using the average method through Gaussian integration [30]. To make a fair comparison, we employ the same single crystal elastic constants as in Ref. [30]: $C_{11} = 59.3$, $C_{12} = 25.7$, $C_{13} = 21.4$, $C_{33} = 61.5$, $C_{44} = 16.4$ (all in GPa at 300 K) and assume sharp interface between grains. The polycrystalline microstructure is subjected to a constant applied strain and the eigenstrain field is assumed to be zero. The calculated effective elastic constants listed in Table 1 agree well with the literature data, which are the average value using Hill approximations [30].

To investigate the temperature effect on the effective elastic properties, we use the single crystal elastic constants from

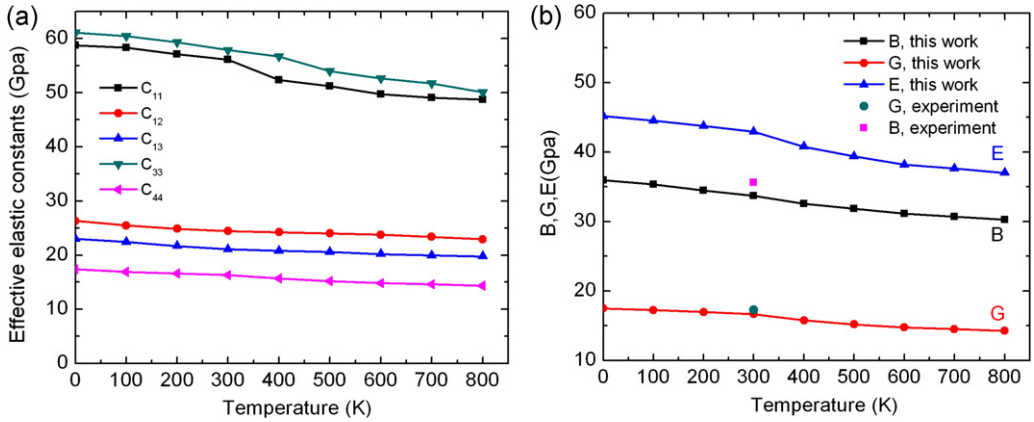

Fig. 2. (a) Calculated effective elastic constants of polycrystalline Mg as a function of temperature using sharp interface model. (b) Temperature dependent effective modulus (*B*, *G*, *E*) of polycrystalline Mg at room temperature, in comparison with experimental measurements [31].

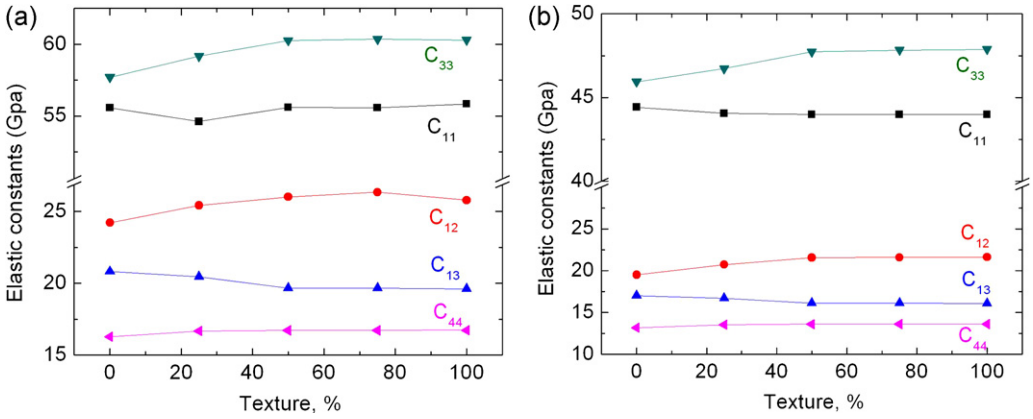

Fig. 3. Effect of the basal texture ($\{0\,0\,0\,1\}$, $\langle 1\,0\,\bar{1}\,0\rangle$) on the computed effective elastic constants using: (a) sharp interface model and (b) diffuse interface model.

first-principles calculations shown in Fig. 1(b) as input. The calculated effective elastic constants are plotted in Fig. 2(a) as a function of temperature, still using the sharp interface model. Generally, these elastic constants slightly decrease as a function of temperature. Among them, C_{11} and C_{33} have larger temperature dependency than C_{12}, C_{13} and C_{44}, which are nearly independent of temperature. This behavior is similar to the single crystal elastic constants as shown in Fig. 1(b). The effective elastic constants obtained at 300 K are slightly different from the values listed in Table 1, due to the different input elastic constants. Comparing with the 5 independent elastic constants of single crystal Mg in Fig. 1(b), the calculated effective elastic constant C_{33} is close to C_{11}, C_{13} is close to C_{12}, and C_{44} is close to $(C_{11}-C_{12})/2$, which demonstrates the behavior of isotropic symmetry with 2 independent elastic constants. The derived bulk modulus (B), Young's modulus (E) and shear modulus (G) are plotted in Fig. 2(b) and exhibit the same temperature dependent behavior. Furthermore, the experimental shear modulus (G) and bulk modulus (B) at 300 K [31] are included for comparison. The shear modulus has a good agreement with the calculated value, while the Young's modulus is slightly larger than the prediction. This is because the input single crystal elastic constants C_{11} and C_{33} from first-principle calculations are smaller than the experimental values.

In the above calculations, all the grains are assumed to be oriented randomly, which means the Euler angles θ, ψ, and ζ are random numbers between 0 and 2π for each grain. In the phase-field method, textures can be easily introduced to polycrystalline microstructures by assigning specific Euler angles to the grain orientation, instead of the random values. The texture in rolled sheet hexagonal metals are commonly represented by $\{h\,k\,i\,l\}\langle u\,v\,t\,w\rangle$, which means that the $\{h\,k\,i\,l\}$ planes of these grains lie parallel to the sheet plane, whereas their $\langle u\,v\,t\,w\rangle$ direction point parallel to the rolling direction [9]. In this work, two representative textures in magnesium alloys will be selected to study the texture effect on the effective moduli: basal texture $\{0\,0\,0\,1\}\langle 1\,0\,\bar{1}\,0\rangle$ and fiber texture $\{1\,1\,\bar{2}\,0\}\langle 0\,0\,0\,1\rangle$, while the latter is the representative recrystallization texture during the columnar solidification process for magnesium alloys. For basal texture $\{0\,0\,0\,1\}\langle 1\,0\,\bar{1}\,0\rangle$ the corresponding Euler angles are $\theta=0.6^\circ$, $\psi=0^\circ$ and $\zeta=60^\circ$, for fiber texture $\{1\,1\,\bar{2}\,0\}\langle 0\,0\,0\,1\rangle$ $\theta=90^\circ$, $\psi=90^\circ$ and $\zeta=0^\circ$ (Bunge system) [9]. By specifying the above Euler angles to a certain number of grains, we calculate the effective elastic constants from a completely random polycrystal (0% texture) to a fully textured polycrystal (100% textured). The calculations are performed using both sharp and diffuse interface models to compare the grain boundary effects.

Fig. 3 shows the variation of effective elastic constants as a function of basal texture $\{0\,0\,0\,1\}\langle 1\,0\,\bar{1}\,0\rangle$, using both sharp interface and diffuse interface assumptions. Comparing Figs. 3(a) and (b), the calculated elastic moduli are smaller in magnitude when we relax the sharp interface assumption and take into account the effect of grain boundaries (Fig. 3(b)). This result stems from our definition of position dependent elastic stiffness tensor in Eq. (1). As expected, there is no significant variation of elastic properties with increasing basal texture, due to the isotropic elastic properties within the basal plane of hexagonal structure, i.e., $C_{11}=C_{22}$. The small variations of the calculated values with different amount of texture are likely due to the grain boundary effect while theoretically they should be completely uniform.

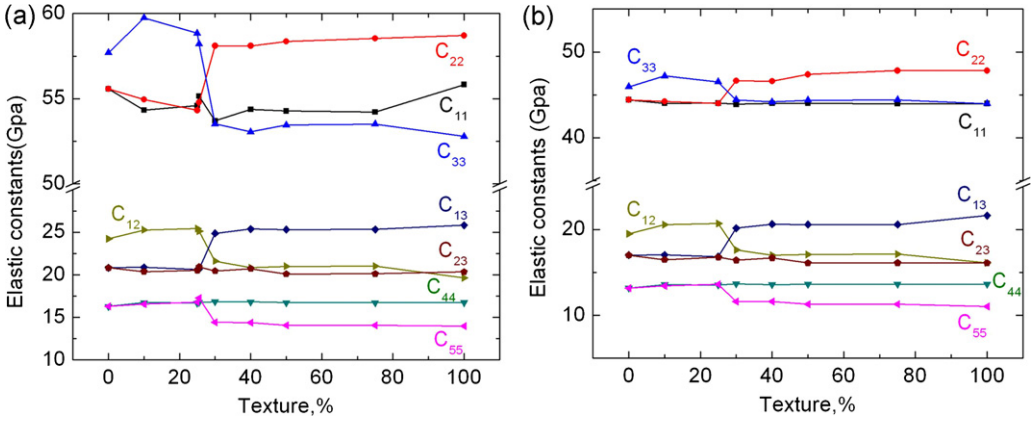

Fig. 4. Effect of the fiber texture ($\{1\,1\,\bar{2}\,0\}$, $\langle 0\,0\,0\,1\rangle$) on the computed effective elastic constants using: (a) sharp interface model and (b) diffuse interface model.

However, when we assign the fiber texture $\{1\,1\,\bar{2}\,0\}\langle 0\,0\,0\,1\rangle$, the effective elastic constants show a pronounced change with increasing texture amount, as shown in Fig. 4. For both models, the elastic constants have a significant change when the polycrystalline has more 25% textured grains. A polycrystal with 100% $\{1\,1\,\bar{2}\,0\}\langle 0\,0\,0\,1\rangle$ fiber texture shows an increased anisotropy and a lower crystallographic symmetry with eight independent elastic constants.

4. Summary

In summary, we employ a phase-field description of grain structures and microelasticity to calculate the effective elastic properties of polycrystalline magnesium. The obtained effective elastic moduli agree well with available experimental measurements. We also examine the texture effect on the effective elastic properties by quantitatively assigning certain amount of texture components into the polycrystalline grain structure. Simulation results indicate that a fiber texture $\{1\,1\,\bar{2}\,0\}\langle 0\,0\,0\,1\rangle$ has a strong impact on the effective properties while the effective moduli are nearly independent of the basal texture $\{0\,0\,0\,1\}\langle 1\,0\,\bar{1}\,0\rangle$. The diffuse interface assumption employed in our model is able to predict the size dependent elastic properties of nanocrystals where the grain size is small and grain boundary effect is significant. The presented approach, combining phase-field description of microstructures and first-principles calculations of single-crystal properties, also provides an efficient way to predict many other effective properties such as piezoelectric constants, magnetic permeability, and thermal conductivity.

Acknowledgements

The financial support from U.S. Army Research Laboratory under contract W911NF-08-2-0064 is greatly acknowledged. The work is also partially supported by NSF under the grant number DMR-0710483 (Chang and Chen). Calculations were conducted at the LION clusters at the Pennsylvania State University and in part supported by Instrumentation (cyberstar Linux cluster) funded by the National Science Foundation through grant OCI-0821527, and in part by the Materials Simulation Center and the Graduate Education and Research Services at the Pennsylvania State University.

References

[1] A. Luo, Materials comparison and potential applications of magnesium in automobiles, in: B.B. Clow (Ed.), Magnesium Technology 2000, Minerals, Metals and Materials Society/AIME, PA, Nashville (TN), 2000, p. 89.
[2] M. Bamberger, G. Dehm, Annu. Rev. Mater. Res. 38 (2008) 505.
[3] T.R.Long, C.S. Smith, Acta Metall. 5 (1957) 200.
[4] L.J. Slutsky, C.W. Garland, Phys. Rev. 107 (1957) 972.
[5] S. Eros, C.S. Smith, Acta Metall. 9 (1961) 14.
[6] E.R. Naimon, Phys. Rev. B 4 (1971) 4291.
[7] E.R. Naimon, T. Suzuki, A.V. Granato, Phys. Rev. B 4 (1971) 4297.
[8] L.F. Magana, G.J. Vazquez, J. Phys.: Condens. Matter 7 (1995) L393.
[9] Y.N. Wang, J.C. Huang, Mater. Chem. Phys. 81 (2003) 11.
[10] W. Voigt, Lehrbuch der Kristallphysik, Teubner, Berlin, 1910.
[11] A. Reuss, Z. Angew. Math. Mech. 9 (1929) 49.
[12] R. Hill, Proc. Phys. Soc. (London) 65 (1952) 349.
[13] T. Dutta, T.K. Ballabh, T.R. Middya, J. Phys. D: Appl. Phys. 26 (1993) 667.
[14] J.E. Gubernatis, J.A. Krumhansl, J. Appl. Phys. 46 (1975) 5.
[15] H. Kiewel, L. Fritsche, Phys. Rev. B 50 (1994) 5.
[16] N.J. Park, H.J. Bunge, H. Kiewel, L. Fritsche, Texture Microstruct. 23 (1995) 43.
[17] J.M.J. den Toonder, J.A.W. van Dommelen, F.P.T. Baaijens, Modell. Simul. Mater. Sci. Eng. 7 (1999) 909.
[18] L.Q. Chen, Annu. Rev. Mater. Res. 32 (2002) 113.
[19] Y. Ni, Y.M. Chiang, J. Mech. Phys. Solids 55 (2007) 517.
[20] G. Laschet, M. Apel, Steel Res. Int. 81 (2010) 637.
[21] S. Bhattacharyya, T.W. Heo, K. Chang, L.Q. Chen, Commun. Comput. Phys. 11 (2012) 726.
[22] S. Bhattacharyya, T.W. Heo, K. Chang, L.Q. Chen, Modell. Simul. Mater. Sci. Eng. 19 (2011) 035002.
[23] S.Y. Hu, L.Q. Chen, Acta Mater. 49 (2001) 1879.
[24] D. Fan, L.Q. Chen, Acta Mater. 45 (1997) 611.
[25] D. Fan, C. Geng, L.Q. Chen, Acta Mater. 45 (1997) 1115.
[26] C.E. Krill, L.Q. Chen, Acta Mater. 50 (2002) 3057.
[27] K. Chang, W.M. Feng, L.Q. Chen, Acta Mater. 57 (2009) 5229.
[28] S. Vedantam, B.S.V. Patnaik, Phys. Rev. E 73 (2006) 016703.
[29] H. Zhang, Ph.D. Thesis, The Pennsylvania State University, 2010.
[30] A.V. Nikishin, D.I. Nikolaev, Crystallogr. Rep. 53 (2008) 493.
[31] P. Sisdodia, M.P. Verma, Phys. Status Solidi A 122 (1990) 525.